CHEMISTRY OF MATERIALS

Perspective

pubs.acs.org/cm

Visualization of Electrochemical Reactions in Battery Materials with X-ray Microscopy and Mapping†

Mark Wolf, Brian M. May, and Jordi Cabana*

Department of Chemistry, University of Illinois at Chicago, Chicago, 60607 Illinois, United States

ABSTRACT: Unlocking the full performance capabilities of battery materials will require a thorough understanding of the underlying electrochemical mechanisms at a variety of length scales. A broad arsenal of X-ray microscopy and mapping techniques is now available to probe these processes down to the nanoscale. The tunable nature of X-ray sources allows for the extraction of chemical states through spectromicroscopy. The addition of phase contrast imaging can retrieve the complex-valued refraction of the material, giving an even more nuanced chemical picture. Tomography and coherent Bragg diffraction imaging provide a reconstructed three-dimensional volume of the specimen, as well as internal strain information from the latter. Many recent insights into battery materials have been achieved through the creative use of these, and similar, methods. Experiments performed while the battery is being actively cycled reveal behavior that differs significantly from what is observed at equilibrium and metastable conditions. Planned improvements to X-ray source brightness and coherence will extend these techniques by alleviating the current trade-off in time, chemical, and spatial resolution.

INTRODUCTION

Beyond the visible consumer electronics applications, energy storage plays a critical role in areas such as manufacturing, transportation, and electricity generation. By some estimates, US industries lose $80 billion each year due to power interruptions, while annual electric vehicle sales are seeing large and consistent increases.[1] Additionally, if renewables are to become the main source of energy production, we will need storage solutions to deal with their intermittent nature. Even with coal and natural gas, fluctuations in demand require that more expensive "peaker plants" be brought online, which could be alleviated if energy from base-load plants can be stored when demand is low. The cheapest energy storage methods, pumped-hydro and compressed-air, are severely limited by the availability of suitable locations. Currently, batteries hold much promise as portable energy storage systems. Batteries contain two electrodes, sites where oxidation and reduction reactions (redox) take place.[2] The fundamental redox chemistry within batteries is nontrivial and governs the practical aspects that are felt by the consumer, such as capacity, cycle life, and power, among others. Therefore, advances in battery technology that yield cheaper, more reliable, and better performing systems will result in large economic, environmental, and geopolitical benefits. A key requirement for achieving this goal is a better understanding of the chemistry underlying these materials, in order to operate as close as possible to their theoretical limits.

Measuring chemical properties with spatial resolution provides a view of the underlying mechanisms that is not available by looking at bulk properties. Electrodes generally adopt a hierarchical structure wherein single crystallites of a redox-active material combine to form agglomerate particles, which are then combined with conductive additives and flexible polymeric binders into a thick (ideally, above 100 μm), porous electrode architecture (Figure 1) where different distributions of components and particle sizes are likely to exist throughout

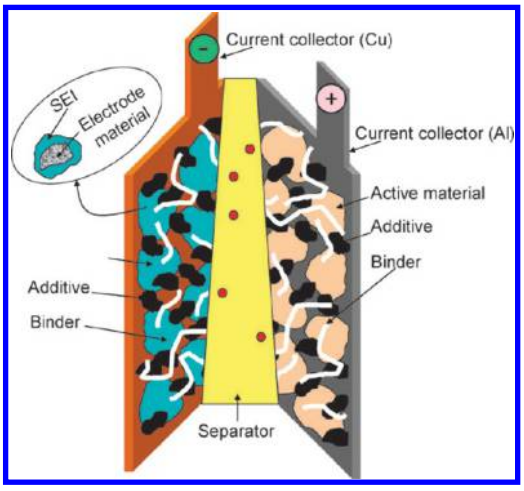

Figure 1. Schematic of a typical battery. The electrodes are made of multiple individual particles that participate in the electrochemical reaction (denoted as "active material"). Reproduced from ref 5 with permission. Copyright 2009 the Royal Society of Chemistry.

Received: December 1, 2016
Revised: March 17, 2017
Published: March 21, 2017

†This Perspective is part of the *Up-and-Coming* series.

DOI: 10.1021/acs.chemmater.6b05114
Chem. Mater. 2017, 29, 3347−3362

the electrode, demonstrated in Figure 2. In addition, the thickness of the electrode introduces asymmetries in the transport of ions (from the electrolyte) and electrons (from the current collector, Figure 2), which are both required in order for the redox reaction to proceed. As a result, a hierarchy of inhomogeneities develops during the phase transformation, both within the electrode[3,4] and within individual particles. These inhomogeneities are kinetic in origin, beyond the changes that would be inherent to the phase transformation within a particle and, thus, prone to vary with the currents to which the battery is subjected. Probing all of these length scales provides clues to meet the high demands placed on current technology.

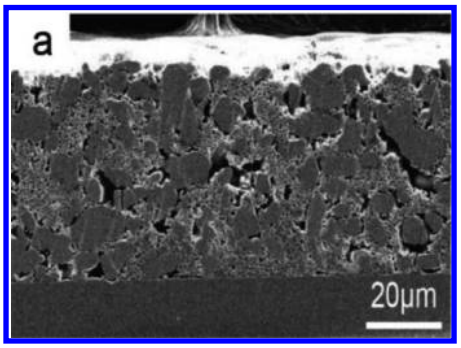

Figure 2. Scanning electron microscope image of the cross-section of a typical battery electrode. Multiple individual particles can be seen that participate in the electrochemical reaction. Reprinted from J. Choi et al. Improved high-temperature performance of lithium-ion batteries through use of a thermally stable copolyimide-based cathode binder. *J. Power Sources* **2014**, *252*, 138−143, with permission. Copyright 2014 Elsevier.

X-rays are able to probe various length scales using a variety of contrast mechanisms. Compared to electron microscopy, another common tool for achieving spatially resolved information from cathode materials, X-rays are significantly less damaging to the material under most circumstances. Additionally, transmission electron microscopy (TEM) in particular has stringent requirements for sample thickness, often below 100 nm. In contrast, the ability to tune the X-ray energies offers flexibility in terms of the ability to measure large objects. This Perspective focuses on the use of X-ray techniques as a means to collect chemical information over various time and length scales. It is biased toward techniques that have already seen applicability in battery science. In other words, it is not meant to be an exhaustive review of all X-ray imaging and mapping techniques that may be available. Readers interested in such reviews are referred to several papers in the peer-reviewed literature.[6−9]

FOREWORD: DEFINITION OF RESOLUTION

Before exploring in detail the different techniques of interest, it is important to define a framework which guides the design of any imaging experiment. This framework is based on the fact that the objective of any chemical imaging experiment is to achieve the maximum resolution along three parameters: space, chemistry, and time (as illustrated in Figure 3). Because advances in spatial resolution are desirable in order to achieve the ultimate objective of visualizing atomic structures, this parameter tends to be the focus of the attention of researchers developing these techniques. However, as will become apparent throughout this perspective, the deepest level of insight into the

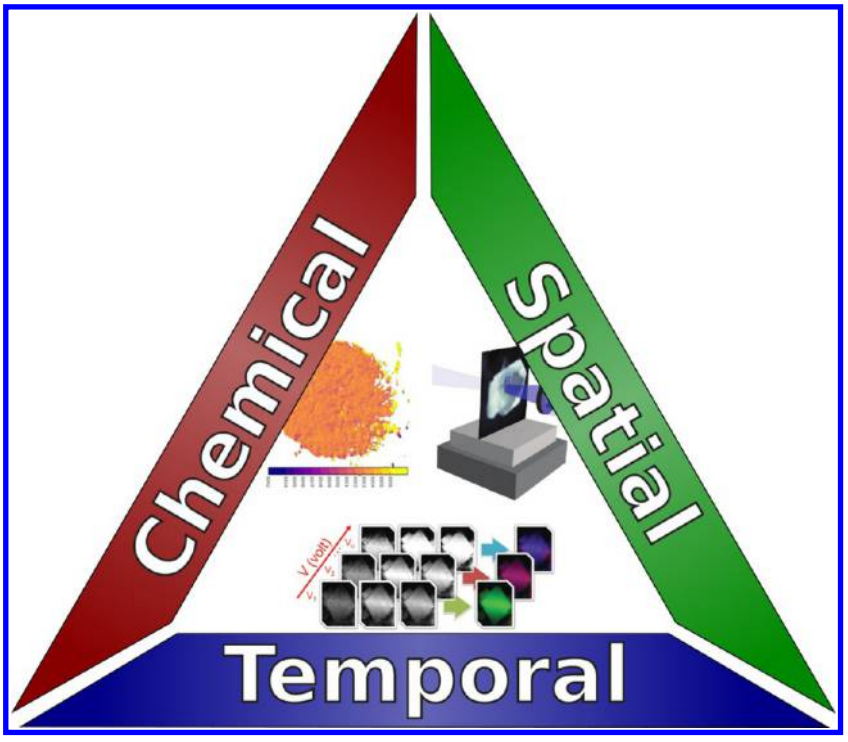

Figure 3. Resolution triangle, showing the trade-off between chemical, spatial, and time resolution. Reprinted in part with permission from Yu et al. Nonequilibrium Pathways during Electrochemical Phase Transformations in Single Crystals Revealed by Dynamic Chemical Imaging at Nanoscale Resolution. *Adv. Energy Mater.* **2015**, 5. Copyright 2014 John Wiley and Sons. Reprinted with permission in part from ref 10. Copyright 2014 Macmillan Publishers Limited.

DOI: 10.1021/acs.chemmater.6b05114
Chem. Mater. 2017, 29, 3347−3362

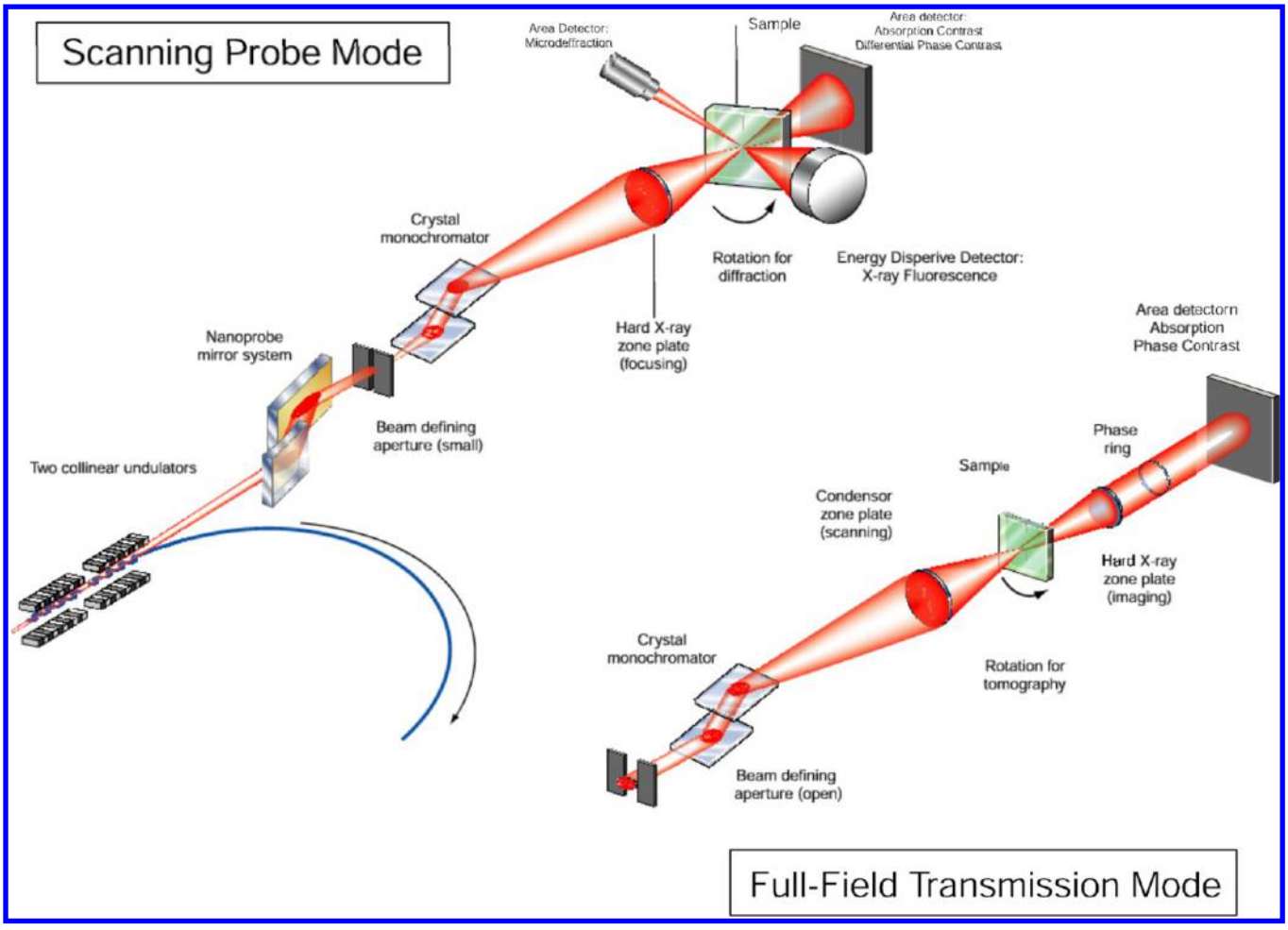

Figure 4. Illustration of experimental configurations for (a) scanning probe and (b) full-field imaging synchrotron hard X-ray microscopy methods. Reprinted with permission from Maser et al. Development of a Hard X-ray Nanoprobe Beamline at the Advanced Photon Source. *Microsc. Microanal.* **2005**, 11, 680−681. Copyright 2005 Cambridge University Press.

electrochemical reactions that determine battery function requires a thorough detection of different chemical states that may often present similar signals, all while operating under an electrochemical stimulus. The latter necessarily implies the importance of temporal resolution so as to acquire multiple data points along the reaction pathway, which may be as fast as seconds. Advances are still needed that push the three parameters forward at the same time. Instead, the current situation forces sacrifices in either of these scales of resolution.

■ X-RAY IMAGING EXPERIMENT

X-ray Sources. X-ray generation is possible by two different means: laboratory sources and synchrotron facilities. The general concept of the lab source is based on tubes under vacuum, containing a cathode that is biased so as to generate and accelerate electrons. These electrons collide with the metallic anode, generating X-rays over a narrow range of wavelengths. The specific wavelengths of the resultant X-rays are dependent on the metal used for the anode. Common laboratory X-ray sources include the sealed X-ray tube and rotating anode generator, which differ on the level of vacuum, seal, and arrangement of the metallic anode.[11]

Synchrotron radiation is also generated from accelerating charged particles but provides higher intensity and better coherence than is currently possible with laboratory sources. Unlike laboratory sources, which are broadly available, synchrotrons require very large areal footprints and, thus, are part of central facilities that are open to users worldwide through a competitive proposal system. The particles, typically electrons, are first accelerated to relativistic speeds, at which point they enter the storage ring of the synchrotron. Beamlines are built tangential to the storage ring so as to utilize X-ray radiation generated when the particles are subjected to centripetal acceleration, either through bending magnets or insertion devices, such as wigglers and undulators. Bending magnets serve two purposes. First, they are placed in such a way that the charged particles in the storage ring are redirected to maintain a proper pathway. Second, each redirection generates X-rays, which are then used in experimental stations. Insertion devices are specialized for generating X-rays and differ from bending magnets in that they are straight sections of the ring that have alternating magnetic fields. Charged particles oscillate through the device, with each oscillation essentially equivalent to a single bending magnet. Therefore, the generated photons can reach higher energies than those generated by bending magnets.[12]

An important distinction between laboratory X-ray sources and synchrotron sources is the nature of the X-rays produced. Synchrotron light sources can generate X-rays at much higher intensity than laboratory sources. Another major difference

DOI: 10.1021/acs.chemmater.6b05114
Chem. Mater. 2017, 29, 3347−3362

between laboratory sources and synchrotron sources is that the optics within a synchrotron create a tunable polychromatic X-ray beam, which can subsequently be set to a narrow energy range through the use of monochromators upstream from the end station. In contrast, laboratory sources only produce a limited range of X-ray energies, which is nontrivial to tune. While some techniques fully utilize the white beam,[13] it is more common to select a single desired wavelength and change it during the experiment. Different energy regimes are defined in the X-ray community. Typically, X-rays with energies below ∼2000 eV are termed "soft", whereas beamlines operating in the "hard" X-ray regime achieve values above ∼4000 eV. The intermediate regime between "soft" and "hard" is often termed "tender". The high intensity, brightness, and tunability render synchrotrons as the preferred light sources for chemical imaging.

Methods of X-ray Microscopy. There are two general modes of X-ray microscopy: full-field and scanning (as illustrated in Figure 4). The operation of a full-field X-ray microscope is similar to a conventional visible light microscope. In a full-field microscope, the X-ray beam is first focused down to a few micrometers. This microbeam illuminates the sample, generating a large field of view. The resulting photons are magnified by a second set of optics before reaching the detector. In this mode, the limit in spatial resolution is set by the detector pixel size and any aberrations in the optics. This method results in large images with fine resolution in a single shot. In contrast, a scanning microscope is based on focusing the beam prior to illuminating the sample. In order to collect frames of view that are larger than the illuminated spot, the beam is subsequently rastered over the region of interest in the sample. In this case, the spatial resolution is determined by the combination of beam and scanning step size. Given the different methods of operation, it can easily be concluded that full-field imaging offers higher image throughput than scanning imaging at the highest possible setting. On the other hand, scanning techniques allow for higher versatility in contrast mechanisms than in full field mode, especially when combinations are desired.

Tomography. Individual images in both full-field and scanning X-ray microscopes are generated in two spatial dimensions. However, the two techniques offer the capability of 3D imaging using tomography. A tomographic reconstruction is achieved by taking a series of two-dimensional projection images while the sample is rotated over 180° (ideally), followed by conversion of these images to a three-dimensional volume. This technique is agnostic regarding the contrast mechanism by which the two-dimensional projections were created, meaning it can be combined with any X-ray microscopy contrast mechanism discussed here. Provided the methodology involves the measurement of transmitted photons, tomography allows for the effects of sample thickness to be removed so that the intensity of each voxel is dependent only on material composition. Since the sample is rotating, precise alignment of the rotation axis is necessary to keep the sample in view.

X-ray Optics. All the techniques discussed here require at least some level of focusing of the X-ray beam prior to, and, in some cases, also after, interaction with the sample. The ability to obtain images at increasing spatial resolution is dependent on the type, sophistication, and quality of the focusing optics.

Compound refractive lenses (CRL) use several lenses in series to focus an X-ray beam. CRLs are made of low atomic number materials to reduce X-ray absorption.[14] Reflective optics are used as well for X-ray focusing. First proposed by Kirkpatrick and Baez in 1948, one common setup is the use of two grazing incidence reflective mirrors that are orthogonal to one another (KB mirrors). This setup allows for the incoming X-ray beam to be focused in both dimensions. Both CRLs and KB mirrors are typically used for hard X-rays.[15]

Diffractive optics are an alternative option. They are predominant in the soft X-ray regime but are also compatible with hard X-ray radiation. Fresnel zone plates (FZP) utilize several concentric rings of alternating opaque and transparent zones, decreasing in width as a function of distance from the center. In this way, the diffracted X-rays from the transparent sections of the optic will undergo constructive interference, focusing to a point. The maximum amount that the beam can be focused is inversely related to the width of the outermost ring. Multilayer Laue lenses (MLL) are similar to FZPs, in that they use zones to achieve focusing. However, MLLs use one-dimensional zones rather than rings. Because of this, they can be synthesized using thin film deposition, which allows for smaller thicknesses than current lithographic techniques.[12,16]

Modern focusing optics typically limit the spatial resolution of the measurement to roughly 10 nm, with MLLs.[17] Focusing optics have an inherent disadvantage that the resultant spatial resolution is dependent on the optic itself. Lensless techniques remove this restriction. Coherent diffraction patterns may be collected and processed using an iterative reconstruction method to produce an image. Thus, the ultimate limit resides in the wavelength of the incoming radiation, also known as the diffraction limit, meaning that spatial resolutions can be achieved that are smaller than the size of the beam on the sample and the nominal resolution of the optics. Techniques derived from this approach are further discussed below.

Detectors. In full-field microscopy, the magnified X-ray image strikes a scintillator where it is converted to visible light. The total energy of this conversion must be conserved, so one high-energy X-ray photon results in hundreds of low-energy visible light photons. This light is then magnified using visible-light microscopy optics onto a detector, usually a charge-coupled device (CCD). Any defects in the scintillator are clearly visible in the resulting intensity images so it is important to collect a reference frame to remove these features. For scanning microscopy, no post-sample optics are required. Instead, a detector measures the transmitted intensity at each raster position. Photomultiplier tubes (PMTs) have a large collection area, low noise, and high gain, making them ideal for this application. In some specific scanning microscopy methods, a two-dimensional interference pattern is needed at each raster position, so a CCD detector is used instead. The dynamic range of the detector is an important factor to consider. CCDs work by exposing a photoactive layer to radiation, which then results in charge accumulation in the underlying structure, to be read out after some time interval. If a single CCD pixel becomes saturated before being read, the area will have artificially low values in the resulting optical depth image. Shortening exposure time can solve this problem; however, the resulting data will have a lower signal-to-noise ratio. A simple solution is to keep the exposure time short and then collect and average multiple frames.

In the specific case of imaging techniques relying on diffracted X-rays (see below), two-dimensional area detectors are common. These detectors capture a two-dimensional segment of the full three-dimensional pattern (also known as the Ewald diffraction sphere). Any crystallites whose

DOI: 10.1021/acs.chemmater.6b05114
Chem. Mater. 2017, 29, 3347−3362

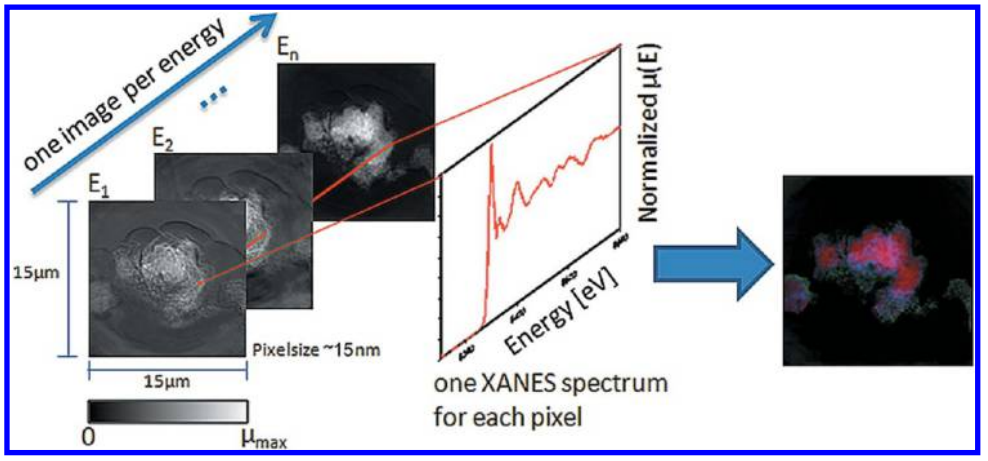

Figure 5. Reduction of TXM stacks to form chemical maps. A full spectrum is extracted for each pixel and used to calculate the chemical state of the material and then converted to a color.[18] Reproduced with permission from ref 18. Copyright 2011 International Union of Crystallography.

orientation produces diffraction vectors landing within this segment will be detected. The exact range depends on the geometry of the experimental setup and the wavelength of radiation used; high energy X-rays cause more diffraction conditions to be detectable in a given area. A one-dimensional pattern can then be obtained by integrating around the resulting diffraction rings.

MECHANISMS OF CHEMICAL CONTRAST

Spectromicroscopy. X-ray microscopy utilizes a multitude of contrast mechanisms. *Absorption contrast* relies on the intensity of the X-rays that penetrate through the material being imaged. From the physical perspective, it involves detecting changes in the amplitude of the incoming X-ray wave after interacting with the sample, most commonly after transmission. Thickness and composition of the material are two major contributing factors to the X-ray absorption. Therefore, through the collection of one signal, both morphological and chemical information can be generated. Since X-ray absorbance depends on interaction with electrons, elements with higher atomic numbers have a higher absorbance. Once the X-ray energy exceeds that needed to promote a core electron in an element present in the sample, a sharp increase in X-ray absorbance is seen, known as an "edge". Therefore, the specific energy value of the transition is indicative of the element and its chemical state (e.g., formal valence state). Each element can potentially have several absorption edges, depending on how many core electron orbitals it has. These edges are named based on the electron energy level they originate from: "K-edge" for $n = 1$, "L-edge" for $n = 2$, "M-edge" for $n = 3$, etc. Spectromicroscopy is conducted at K- and L-edges. In the specific case of a K-edge spectrum, two regions can be distinguished: XANES (X-ray absorption near-edge structure) and EXAFS (extended X-ray absorption fine structure). XANES provides information on oxidation states while EXAFS provides information on local atomic structure and neighboring atoms. In practice, collection of EXAFS data imposes data acquisition requirements that are currently unrealistic in spectromicroscopy.

Fluorescence contrast is similar to X-ray absorption in that it relies on electron excitation. The fluorescence signal, however, comes from the subsequent light re-emission. For the element of interest, the X-ray energy can be set just above the absorption edge. If the incoming X-ray energy is set above the absorption edge for several elements in a sample, they will all fluoresce at different energies. Thus, fluorescence imaging can be advantageous over X-ray absorption for gathering elemental distribution, especially in dilute samples. If the energy is scanned below and through the edge, fluorescence detectors can also be used to produce X-ray absorption spectra, in a manner that is compatible with spectromicroscopy. This approach was recently demonstrated in battery materials.[19]

Phase contrast imaging is an alternative to absorbance: the changes of the observed phase of X-ray waves, as opposed to their amplitude, are monitored. These changes are observed as the thickness/density of the sample changes. In order to resolve the differences in the phase shift, δ, the detector is generally placed far behind the sample. Phase contrast imaging is advantageous as it is more sensitive than absorption contrast and can therefore utilize lower X-ray intensities. For this reason, phase contrast is often used to study materials that do not absorb strongly or that are sensitive to radiation damage. A drawback for some, phase contrast imaging heavily relies upon a highly coherent X-ray source, as well as a sophisticated detector. A complex-valued refraction spectrum can be acquired using phase contrast by collecting data over a range of energy points. This information will also be dependent on the electronic structure of the sample, but due to its complexity, this method of spectromicroscopy remains under development.[20]

In spectromicroscopy, whether full-field or scanning, the same field-of-view is imaged repeatedly while the energy of the incident beam is changed over an absorption edge of the element(s) of interest. The resulting frame-stack provides a full absorbance and/or phase spectrum at each pixel. These spectra are then processed into a scientifically meaningful quantity to generate chemical maps of the field-of-view. In order for pixel-wise spectroscopic conclusions to be valid, it is critical that the images be properly aligned with one another, which is rarely the case with raw data sets. The next step in the analysis involves normalization of the spectra relative to the background optical depth. As X-ray energy increases, the transmission of all materials increases as well. Correcting for this effect improves the reliability of analysis methods that involve decomposing the spectra into components of known materials.[21]

Conversion of the resulting absorbance spectra to some figure of scientific merit depends in large part on the question being addressed by the experiment. A common goal is to map the distribution of certain elements. This goal can be

DOI: 10.1021/acs.chemmater.6b05114
Chem. Mater. 2017, 29, 3347−3362

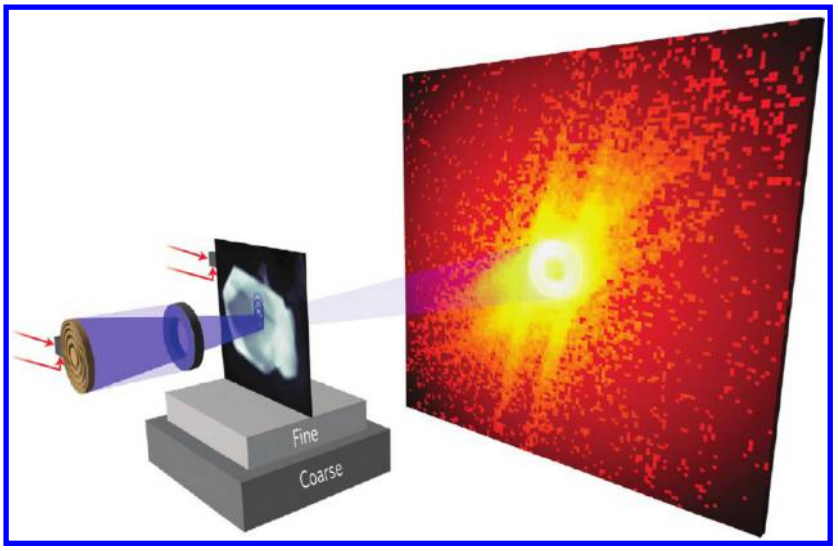

Figure 6. Schematic of a soft X-ray ptychographic microscope. An incoming X-ray beam is focused onto the sample by a zone plate and order sorting aperture. The coherent diffraction pattern is collected by a CCD.[10] Copyright 2014 John Wiley and Sons. Reprinted with permission from ref 10. Copyright 2014 Macmillan Publishers Limited.

accomplished by collecting two frames per element: one above and one below the absorption K-edge. By comparing these "edge-jump" values for the elements in question, their relative concentrations can be calculated.[22] Alternatively, generating spectroscopic maps involves reshaping the data to give an array of spectra, each one corresponding to a pixel in the final map. This outcome is accomplished by "looking through" a frame-set along the energy dimension and flattening along the image dimensions, as illustrated in Figure 5. In theory, any analysis that is performed on a bulk spectrum can be done on a single-pixel spectrum. In practice, there are generally a lot of spectra to be analyzed; a set of 1024 × 1024 frames contains over 1 million spectra to be processed. This situation means that analysis cannot rely on human intervention. If prior knowledge of the presence and distinct spectra of multiple phases in the data set is available, their signals can be decomposed.[10,23,24] If the component spectra are not known, which is often the case, a variety of signal processing techniques, such as *independent components analysis* (ICA)[25] or *Bayesian* methods,[26] can be used to approximate them and extract the relative proportions of each component.[27,28] Care must be taken, however, since many of these methods assume properties of the data that are not necessarily true. *Principal components analysis* is a common alternative to ICA that has seen application in spectromicroscopy of battery materials.[10,29] Another approach involves the use of numerical methods to directly map some property of the spectrum. This approach is most effective if an argument can be made that the directly calculated value correlates strongly with some change in the properties or state of the material. For example, the oxidation state of nickel in several layered battery cathode materials is accompanied by a shift in the edge and whiteline positions of the corresponding K-edge spectrum to higher energies;[30] extracting and mapping the whiteline position for each pixel's spectrum can provide a map that approximates the oxidation state of the metal and consequently the state-of-charge of the material. Care must be taken to account for small variations in absorbance across the two or three largest absorbance points which are due not to the sample but to background or spurious signals.

Bragg Diffraction Microscopy. Bragg X-ray diffraction (XRD) provides complementary information to spectroscopy. Rather than observing electronic transitions, it provides a measurement of the distance between crystalline planes (d-space) within a material. This crystallographic information means that unit cell parameters, atomic defects, strain, and microstructural information on the coherent domains are available. Of particular interest in the context of this discussion is the ability to interpret the unit cell dimensions as a given chemical composition if prior knowledge of the system exists. In order to observe diffraction from a material, the Bragg condition must be satisfied, in which a particular X-ray wavelength, crystal spacing, and orientation must be met. A conventional XRD experiment holds the X-ray wavelength constant, while altering the incident and detected beam angles. In contrast, energy dispersive X-ray diffraction (EDXRD) holds the orientation constant and varies the wavelength. As a result, no goniometer is required, and the variation in wavelength can be used to profile the depth of the sample, but extracting physical quantities from the resulting data is less straightforward.[31,32] Once a diffraction pattern is obtained, crystallographic parameters can be extracted and used for mapping. The data generated in Bragg diffraction microscopy experiments can be treated very similarly to those collected during spectromicroscopy. Each mapping position is equivalent to a pixel in an X-ray micrograph, and a series of frames are collected at different scattering vectors, q. Generally, the spatial dimensions are the slowest-changing in diffraction mapping, whereas they are the fastest (or even simultaneous) in microscopy; this distinction does not change the structure of the data in a significant way. However, it does obviate the need to align each image. Rather than a full absorbance spectrum at each location, these experiments generate a diffractogram at each position. Theoretically, a researcher can analyze the two-dimensional diffraction pattern at each position; often, the 2D patterns are integrated to form the more traditional 1D diffractograms. From here, a refinement can retrieve crystallographic parameters, such as unit-cell dimensions, strain, or phase ratios.

The Ultimate Frontier: The Lensless Microscope. Phase contrast and Bragg diffraction are combined in coherent

DOI: 10.1021/acs.chemmater.6b05114
Chem. Mater. 2017, 29, 3347−3362

diffractive imaging (CDI). A single particle fulfilling the Bragg condition is illuminated by a coherent X-ray beam that is larger than the particle. The detector is placed far away from the sample, so that it can collect fringes of the diffracted beam. An iterative algorithm is used to reconstruct an image from the phase information in the fringes of a three-dimensional diffraction pattern.[33] This methodology decouples spatial resolution from the characteristics of any focusing optics used. In other words, as a lensless technique, the process of generation of images does not suffer from lens aberration and thus allows for very high spatial resolution approaching the diffraction limit, under 10 nm in some cases.

Ptychography is another lensless technique which also relies on collecting the full diffraction pattern using coherent diffraction. Unlike CDI, this is a scanning technique; small spots are collected in such a fashion that they spatially overlap on the sample as demonstrated in Figure 6. Similar to CDI, ptychography utilizes an iterative algorithm to reconstruct an image from the diffraction patterns. As a result, the ultimate spatial resolution is, to a large extent, independent from the size of the beam used to collect the overlapping patterns. Artifacts from the reconstruction process sometimes manifest as high frequency bands alongside sharp edges in the specimen. Since this technique is driven by an interference pattern, the best reconstructions are obtained from strongly scattering materials. Ptychography has also been performed in tomographic mode,[34] but this methodological area is still in its infancy. As an added bonus, the reconstruction produces both the real and imaginary components of the object image. By comparison to an area with no material, the fully complex refractive index can be calculated. Exploiting the complex-valued nature of this technique is a relatively unexplored area.

Visualization and Colormaps. Turning a large data set into a two-dimensional image is a task of increasing difficulty as the number of dimensions increases. For applications with two spatial dimensions, images are generated by data reduction as described in the preceding sections. The relationship between values and colors is known as a "colormap" or "lookup table". The choice of colormap can have subtle effects on how the data are interpreted. In general, human vision associates the brightness of a color with the value it represents, regardless of its hue. Therefore, an effective colormap translates high values to high-brightness colors and low values to low-brightness colors. Rainbow colormaps, such as *jet*, do not meet this criterion and should be avoided for representing sequential data. Jet contains bands of high and low brightness that are perceived as sharp gradients in the data that do not actually exist. Perceptually uniform colormaps, such as *viridis* for Matplotlib and *parula* for Matlab, are designed to avoid this problem. Additionally, viridis was tested against color blindness and ensures that data display properly to people in this category.

Projecting data with three spatial dimensions onto a two-dimensional canvas can be done with any one of several visualization tools. Typically, certain features in the data are of interest, such as internal fractures within particles or the distribution of certain elements. Successful visualization usually requires additional analysis steps that identify and highlight these features while making the surrounding material partially transparent. Avizo (FEI) is a popular commercial software package specifically designed to work with tomography data: it contains a number of filters that allow the data analysis to be performed within one piece of software. An additional Avizo package can be purchased that allows it to handle data sets that do not fit entirely into main memory, which is often the case for tomography. An alternative is Paraview (Kitware Inc. and Los Alamos National Lab), a general purpose visualization platform that is highly extensible, allowing python plugins to be run from within the application. Paraview has the additional benefit of being free and open source. For quick inspection of tomographic slices, ImageJ provides the Volume Viewer plugin (included in the FIJI distribution), which is more straightforward to use than either Avizo or Paraview, but has fewer features.

EX SITU VERSUS OPERANDO

To a large extent, electrochemistry is most interesting when away from equilibrium. As electrochemical devices, batteries are useful during operation, which is inherently under kinetic control. While the kinetic states are determined by the thermodynamics of the system, metastability is more prominent under electrochemical conditions than in other classical chemical environments, such as high temperatures. This prominence also implies that the probability of producing kinetic states that are only weakly metastable is high. In fact, the problem of self-discharge, common in certain batteries, is precisely the product of equilibration of a metastable charged state. As a consequence of the pervasive kinetic control, ex situ measurements, which rely on harvesting samples from a cell at a desired chemical state, introduce uncertainty when the goal is to describe relevant states under working conditions. Nonetheless, if caution is applied, and due to their simplicity, these measurements can still provide valuable guidance,[24] mainly because they do not critically suffer from constraints in measurement time and, thus, can result in the highest data quality. Ultimately, operando measurements of battery reactions are preferred because of the growing body of evidence showing that there are many cases where the state within an operating battery is different from what is observed once the cell is disassembled,[35,36] especially when high rates are employed. For this reason, researchers developing novel methods of imaging should have motivation to enter a path that results in means to operando analysis. At this point, given certain confusion in the field, it is worth clarifying that we consider operando measurements to be a small subset of in situ science. The condition *sine qua non* for an operando experiment is that the cell is not stopped to collect data unless the goal is specifically to measure equilibration phenomena.

While operando measurements are preferred and should be pursued, they can present several challenges of varying degrees of difficulty. The setup must allow photons to pass through both the sample and the apparatus with very little disturbance to the signal from the apparatus itself. First and foremost, X-ray absorbing materials have to be minimized in order to ensure sufficient signal reaches the detector. Ideally, supporting materials containing heavier elements should be removed or made sufficiently thin so as to minimize their effects. Another challenge is avoiding X-ray induced damage to supporting materials, such as the polymer binder often used in the construction of cathodes. Maintaining adequate stack pressure may also be important, depending on the nature of the experiment.[37] Additionally, the possibility of deleterious effects of X-ray exposure on the behavior of cathode materials is not completely understood. One possibility is to use very high energy X-rays, which can penetrate the casing material[38] and are less damaging. This strategy is valid for some diffraction

DOI: 10.1021/acs.chemmater.6b05114
Chem. Mater. 2017, 29, 3347−3362

experiments but cannot be applied to spectroscopic imaging since specific energies at which the X-ray beam is absorbed are required.

In situations where high-energy X-rays are not possible, a transparent window is necessary. Beryllium is a typical choice, but its use introduces stringent handling requirements due to its high toxicity, especially in the dispersible form that is generated, for instance, during machining. It also oxidizes relatively easily, making it unsuitable for high-voltage battery applications. Silicon nitride is an appealing option since it can be purchased commercially in prefabricated windows down to tens of nanometers in thickness. At these thicknesses, it also does not have any noticeable morphological features, making it suitable for X-ray microscopy techniques. However, they are very fragile due to their thickness. Polyimide (Kapton) film has found widespread use in operando diffraction experiments, despite the fact that it also introduces an amorphous contribution to diffraction patterns. It has relatively high transmissivity, is easy to fabricate, and is chemically inert. Unfortunately, it cannot ensure a complete seal, and like many other plastics, it often contains filler particles which are heavy enough to become visible in a microscopy experiment, interfering with observations and, thus, rendering it unsuitable. Amorphous carbon can also be used. A large advantage here is its electrical conductivity, which eliminates issues of electrochemical inactivity of the material behind the window. Since it is made entirely of carbon, it also interacts only very weakly with X-rays, so it induces minimal signal attenuation. However, it is difficult to fabricate and can react under certain conditions, such as at very high potentials or against lithium metal. The AMPIX electrochemical cell, developed by Argonne National Laboratory, is an example of a cell with amorphous carbon windows that fits the requirements of an operando X-ray experiment. The cell design (illustrated in Figure 7) ensures good stack pressure as well as electrical conductivity, closely mirroring coin cell conditions.[37,39] Even more sophisticated cells are needed when using low energy, soft X-rays, where the sample volume must be small to avoid excessive absorption of the signal by the sample. In this case, designs that rely on microfabrication have recently been demonstrated.[36]

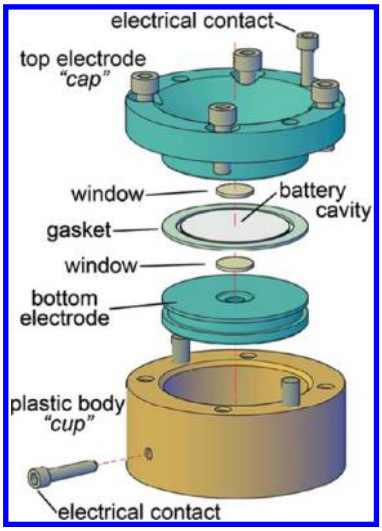

Figure 7. Schematic of AMPIX electrochemical cell.[39] Reproduced with permission from ref 39. Copyright 2012 International Union of Crystallography.

Operando measurements create the most severe challenges to an imaging experiment when considering the three scales of resolution above, namely, spatial, chemical, and temporal. Many battery reactions span several hours, but the need to build a reaction pathway means that it is desirable to collect at least five data points during the reaction. This goal imposes restrictions on the time available to complete an image containing the desired chemical information, at the desired level of spatial resolution. Unfortunately, all modes of chemical contrast require collecting multiple frames for the same reaction state to reconstruct a map of the species present in the field view. Using XANES microscopy as an example, chemical resolution is achieved by collecting frames at a large number of energies, with the limit being set by the precision of the upstream optics. In the particular case of scanning techniques, spatial resolution requires the use of the smallest possible step size to raster the field of view, meaning that a similar trade-off emerges in that the acquisition time is directly affected by this parameter. Additionally, increasing the collection time for each frame will improve the signal-to-noise ratio and improve the accuracy of the data, again at the expense of longer acquisition times for a full frame-set. In practice, the most common choice is to minimize the number of points to obtain some level of chemical resolution in the individual frame-set, whether scanning energy (spectroscopy) or a beam−sample−detector angle (diffraction). This approach strongly relies on prior knowledge of the chemical species involved during the reaction, so that energies or angles are chosen at which signals between these species differ the most. Such prior knowledge is typically acquired through XAS or XRD measurements of the bulk average, as opposed to spatially resolved regions. In the case of the spectroscopy of transition metal species, a change of one unit in the formal oxidation state translates into a displacement of the signals of a few electronvolts, which renders the method viable. Challenges arise when the changes between species are small, for instance, when compounds exist at redox states intermediate between end members. The strategy also inherently lends itself to misinterpretation if previously unknown or unexpected states form in the measurement, especially if they are related to the known, expected species. The local character of an imaging measurement means that the limit of detection of minority species increases with respect to a data set gathered from the bulk average, especially if they accumulated in specific regions of the image. All in all, it is important to be aware of the compromises made to avoid overanalyzing data. Since the field of X-ray imaging is vibrant and constantly pushing the boundaries in resolution, it is likely that these limitations will be alleviated with time, creating exciting opportunities for rich insight into battery operating conditions.

APPLICATIONS OF X-RAY IMAGING TO PROBLEMS IN BATTERY RESEARCH

In this section, we describe representative case studies that serve to highlight the power and versatility of X-ray imaging to elucidate phenomena occurring in battery materials. This section is not meant to be exhaustive, mostly focusing on examples of materials for Li-ion battery electrodes, with an emphasis on those containing transition metals. The reason for the choice of Li-ion devices is that they are the most pervasive battery systems in the research literature (aside from being the most commercially relevant), with examples available that fully exploit the current capabilities in X-ray imaging. These capabilities are not dependent on the device and, thus, can

DOI: 10.1021/acs.chemmater.6b05114
Chem. Mater. 2017, 29, 3347−3362

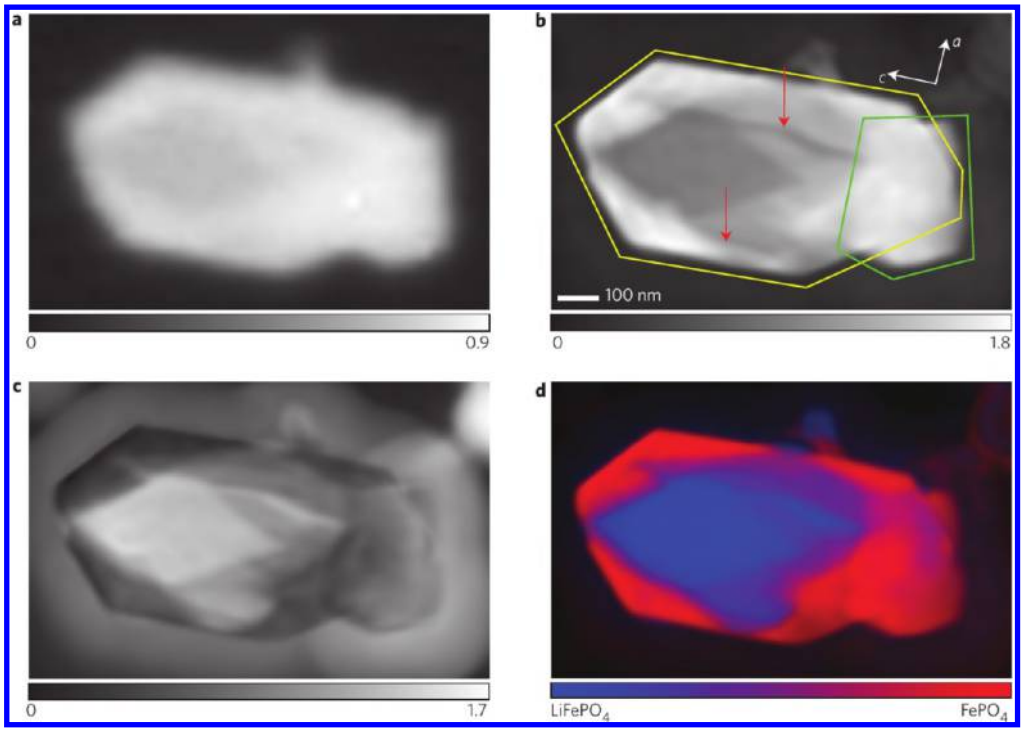

Figure 8. (a, b) X-ray microscopy of partially delithiated $LiFePO_4$. Optical density maps from STXM (a) and ptychography (b) at 710 eV, showing maximum absorption contrast between the end members. The spatial resolution of the STXM is not adequate to visualize the presence of multiple particles, which are outlined in the ptychographic image, and cracks along the crystallographic *c* axis, which are indicated by red arrows (the *a* and *c* crystallographic axes are indicated by white arrows; the *b* axis is parallel to the X-ray transmission). (c) Phase of the ptychographic reconstruction at 709.2 eV, showing maximum relative phase shift between the end members. The halo around the particle is carbon contamination. (d) Colorized composition map calculated by principal component analysis, clustering, and singular value decomposition of the full complex refractive index.[10] Copyright 2014 John Wiley and Sons. Reprinted with permission from ref 10. Copyright 2014 Macmillan Publishers Limited.

be applied to many other battery problems. Indeed, studies of other battery systems with these techniques exist in the literature, exploiting the same features discussed below. For the sake of conciseness, only the chemical identity and a brief mention of the insight gained by the imaging of each electrode material will be presented. For an extensive discussion of the current body of knowledge of electrochemical reactions in the battery materials discussed here, the reader is referred again to reviews available in the peer-reviewed literature.[40,41] Selected applications are grouped by contrast mechanism. X-ray imaging at one or two energies close to an absorption edge can be used to elucidate morphology or elemental distribution, respectively. While these approaches can provide highly valuable information, chemical imaging generally provides increased insight.

Morphology. Absorption imaging at a single X-ray energy provides a direct look at the internal morphology of the material. The short acquisition times and relatively straightforward technical requirements mean that high temporal resolutions can be achieved. For instance, full-field X-ray microscopy has been used to visualize the fate of the components of a battery during thermal runaway with a time resolution of 800 μs.[42] The result was a high frame-rate movie, with no chemical contrast, showing the initial distortion of electrode layers followed by gas formation and finally the catastrophic structural failure of the cell.

Tomography solves a common problem where interpretation of two-dimensional imaging data is confounded by the fact that the measured intensity at each position is a projection through the entire specimen. Tomographic imaging of batteries can even be achieved with laboratory X-ray microscopes.[43] The imaging of electrode morphology can reveal useful information regarding electrode performance. For example, the novel use of a heat-transfer model to extract tortuosity and porosity data from three-dimensional electrode volumes revealed significant anisotropy and heterogeneity in the pore structure, generating unique new inputs for continuum models with the goal to explain and predict electrode behavior.[44] Even when no direct chemical information is obtained, this technique can still illuminate details of the underlying mechanism of electrochemical reaction. In conversion reactions, mixtures of relatively heavy metallic particles and Li_2O are formed.[45] Since the differences in attenuation coefficients of the different species are quite large, quantification of changes in contrast in the image can be used to create pseudochemical maps. This approach is relatively fast, since data collection still occurs at only one X-ray energy. The idea was first exploited by Ebner et al. to study the reduction of tin oxide to tin with microscale spatial resolution. A core−shell mechanism was observed, combined with insight into crack initiation and growth. They also compared particle-level volume changes and their relationship to the expansion of the electrode as a whole. They found that the particles expand beyond the tolerance of the supporting matrix, which has implications for the reversibility of the reaction.[46] A similar approach was applied to nanoscale imaging of individual tin oxide particles, generating new details on particle fracturing and pulverization.[47] This single-energy approach to acquiring chemical contrast is only valid for three-dimensional imaging, since, in two-dimensions, the intensity of a given pixel is heavily influenced by the thickness of the sample at that point. Another limitation is that the majority of reactions

DOI: 10.1021/acs.chemmater.6b05114
Chem. Mater. 2017, 29, 3347−3362

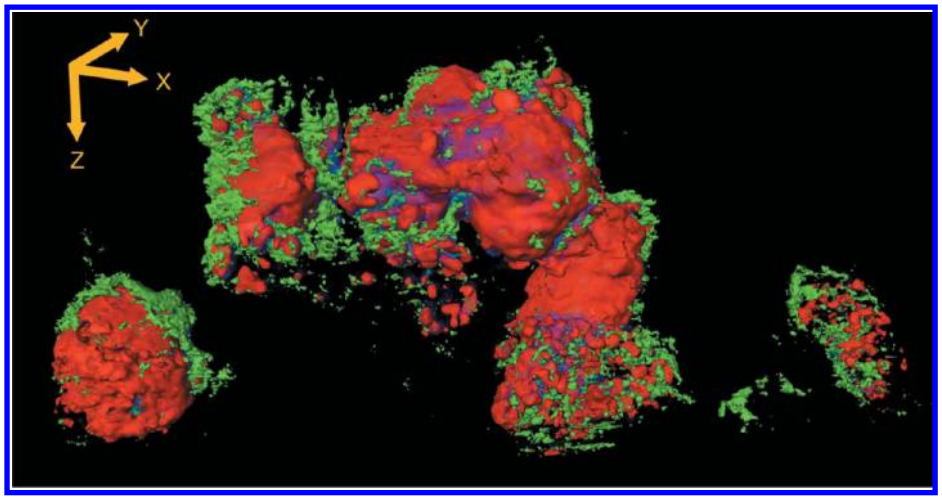

Figure 9. Reconstructed three-dimensional XANES tomography perspective rendering of three-dimensional data set of NiO cathode.[18] Reproduced with permission from ref 18. Copyright 2011 International Union of Crystallography.

of interest in batteries involve compounds that do not show significant differences in attenuation coefficient. In these cases, tomographic techniques with chemical contrast are needed.

Elemental Distribution. Several experiments highlight the ability of X-ray imaging to track the distributions of specific elements in battery materials. Migration of transition metals after one cycle was seen by X-ray absorption tomography.[48] Specifically, the authors discovered depletion of the transition metals at the surface of the particle, accompanied by manganese segregation. Another example used this technique to track transition metal distribution across multiple cycles in a particle of mixed transition metal oxide $LiNi_{0.4}Mn_{0.4}Co_{0.2}O_2$.[49] The authors associated improvements in cycling performance with the existence of an excess of manganese and a depletion of cobalt and nickel at the surface of the particles. The improvement was rationalized through a lower extent of irreversible conversion of nickel-containing layered oxide domains to a reduced rock-salt phase, which is known to be detrimental to charge transfer at the surfaces in these materials.[50]

Spectromicroscopy. Many of the materials used for battery cathode materials do not show significant changes in absorbance between the various states encountered during operation, limiting the scope of the morphological and elemental-distribution techniques. X-ray absorbance spectroscopy provides a direct measure of the chemical state of individual elements. Therefore, it can be used to track the oxidation state of the electrochemically active species. This approach is not limited to a specific technique: it has proven insightful using hard and soft X-rays, K and L absorbance edges, full-field and scanning microscopes, and in two-dimensional and tomographic imaging modes.

Hard X-ray full-field microscopy has seen rather broad applicability to questions in battery research. As an example, it has effectively been demonstrated to locate delithiation domains in olivine-type $LiFePO_4$ microcrystals, and subsequent morphological events, such as fracture, were identified.[29] However, the spatial resolution of a hard TXM, ∼30 nm, did not allow for a specific correlation between chemical domains and fracture points. To achieve this knowledge, soft X-ray absorption spectroscopy coupled with ptychographic microscopy was required in order to gather information at the highest spatial resolution possible today. Yu et al. investigated how crystal size impacts the transformation of $LiFePO_4$ to $FePO_4$.[24] Chemical maps were successfully produced for particles ranging from <100 nm to several micrometers in length. The high spatial resolution achieved in these ptychography measurements, ∼10 nm, finally revealed the correlation between chemical states and physical artifacts, such as cracks. Indeed, comparison of ptychographic imaging with conventional scanning spectromicroscopy highlights the increase in the sharpness of the images, which makes spatial correlation possible. Panels a and b of Figure 8 show the extent of improvement.[10] The work demonstrated that reducing the size of $LiFePO_4$ particles resulted in less extensive fracturing while the distribution of reaction products was very similar, which was taken as an indication of the superior electrochemical performance from $LiFePO_4$ nanoparticles.[24]

Combining tomography and XANES microscopy generates a rich data set that provides a window into the chemical environment at every point in the specimen. Meirer et al. used 3D XANES to probe the conversion of NiO to Ni metal in a partly reduced electrode (Figure 9).[18] By comparing the spectra to known reference materials, they assigned each voxel (3D pixel) to either NiO, Ni metal, or a 50:50 mixture of the two. Additionally, they analyzed virtual slices through the three-dimensional particle to determine how the chemical states were distributed. They found significant inhomogeneities across the particle that depended on its size, as well as evidence of fracturing caused by volume expansion during the reaction. In this case, fracture was revealed as the enabler of the phase progression into the particle, which critically relies on microstructural formatting to reach completion.

Performing X-ray spectromicroscopy operando has the ability to provide insights that are not available with other techniques. The first demonstration of operando measurements using a full-field technique involved the study of the reduction of CuO particles inside a coin-cell modified with Kapton windows.[51] A distinct shell of reduced copper metal was seen surrounded by an unreacted CuO core, along with an intermediate Cu_2O phase. A further iteration of this coin-cell design was developed by Yu et al. and used to study $LiMn_2O_4$ spinel crystals. In order to improve resolution across the board, the emphasis in the design was placed on minimizing the thickness of absorbing materials, such as aluminum, and, for instance, it relied on 1 μm thick silicon nitride windows. The design was applied to the

DOI: 10.1021/acs.chemmater.6b05114
Chem. Mater. 2017, 29, 3347−3362

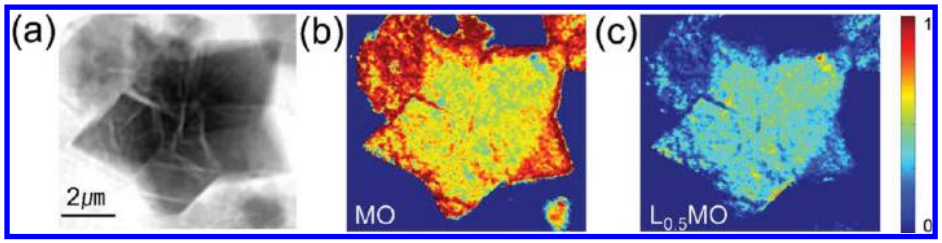

Figure 10. Preferential growth of Mn_2O_4 along cracks at 4.09 V. (a) Inverted optical density image collected at 6700 eV. Heat maps where color contrast scales with the ratio of spectral standards of (b) Mn_2O_4 and (c) $Li_{0.5}Mn_2O_4$ in each pixel. Reprinted with permission from ref 53. Copyright 2014 John Wiley and Sons.

study of the transformation $Li_2Mn_2O_4 \rightleftharpoons LiMn_2O_4 \rightleftharpoons Mn_2O_4$.[52] During the experiment, the authors found significant local effects in the oxidation of the particles, wherein oxidized $LiMn_2O_4$ regions formed and propagated through the crystal. Additionally, a reduced tetragonal $Li_2Mn_2O_4$ phase persisted at potentials well above its predicted stability, according to the phase diagram, leading to a nonequilibrium coexistence with highly oxidized phases. These observations would probably not have been possible under ex situ conditions, where the chemical states are expected to equilibrate. At higher potentials, several cracks in the crystals were seen that correlated with preferential oxidation to the fully delithiated Mn_2O_4 phase, as seen in Figure 10. The authors speculated that these cracks provide additional, fresh interfaces to facilitate phase transformation.[53]

Sustained technical insight into battery reactions from operando spectromicroscopy followed these two studies. A study of $LiFePO_4$ provided details about inhomogeneities in the distribution of oxidized materials between multiple particles.[54] Li et al. studied FeF_3 and showed that the capacity loss seen in this material is due to incomplete conversion from Fe to Fe_3^+ during charging.[21] Beyond Li-ion, another example further elucidates the role of oxygen species in lithium−air batteries. Olivares-Marín et al. looked at the formation of surface barriers, similar to the solid−electrolyte interface, on a carbon substrate. By examining the oxygen K-edge, they showed a relationship between particle morphology and the preference for forming carbonate, peroxide, and superoxide species.[55] The authors argued that the reactive and short-lived nature of some of these oxygen species ensures that meaningful results cannot be obtained without operando measurements.

A significant advance in the quality of operando spectromicroscopy recently occurred thanks to advances in the design of cells brought about by microfluidics. The use of these cells is nicely exemplified by a study of the spatial dynamics of $LiFePO_4$ particles during the electrochemical reaction using soft X-ray scanning TXM.[36] The reliability and control afforded by the microfluidic design enabled the collection of chemical images at a variety of rates while gathering meaningful electrochemical data. Linear combination fitting was used to create maps of lithiated and delithiated material. It was found that the pathways upon lithiation and delithiation were strikingly different depending on the conditions of cycling. Thanks to the quality of the data, the authors were also able to extract the current density for actively (de)intercalating pixels. They found a strong dependence of the exchange current density (j_0) and the degree of lithiation (x in Li_xFePO_4), as shown in Figure 11. Heterogeneities were amplified by this positive feedback mechanism during lithiation and suppressed during delithiation.

The only available example of operando chemical imaging in three dimensions highlights the challenge of interpreting two-

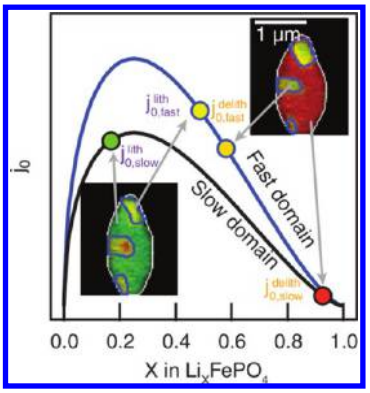

Figure 11. Relationship between measured exchange current density and degree of (de)lithiation. Because the skewed j_0 peaks at $x \approx 0.25$, the value of j_0 for the fast domains is several times that of j_0 for the slow domains during delithiation, but the two quantities are comparable during lithiation. Reprinted with permission from ref 36. Copyright 2016 AAAS.

dimensional projection images directly. Wang et al. collected a 46-point spectrum across the iron K-edge of a $LiFePO_4$ cathode particle and developed a run-out correction system to enable automated tomography. In order to accommodate the significant overhead in time required to acquire 2D images at different energies and angles, the battery was charged extremely slowly (10−100 times slower than would be realistic). Nonetheless, the insight collected was noteworthy, with the advent of a clear core−shell structure, as shown in Figure 12. When considering two-dimensional projections from only one angle, it appeared as though a mixed state existed between the lithiated and delithiated material. Tomographic reconstruction revealed this mixed state to be an artifact of the projection process, as it is not present anywhere in the particle.[23]

■ DIFFRACTION IMAGING

Even though the chemical oxidation state is of primary interest in electrochemical reactions, it is not the only factor affecting performance: structural changes can have a significant impact on the kinetics of the underlying transformation. For example, they are meaningful indications of the presence of misfit strains during transformation, which can lead to the fracture events detected by imaging above.[56] These strain effects are not captured when measuring oxidation state but are well suited to investigation by diffraction-based techniques. As a result, the applications presented here nicely complement the absorbance-based chemical imaging presented above.

Little work has been done on diffraction mapping of lithium-ion cathodes. The most well-known example comes from Liu et al.,[57] where the authors used synchrotron radiation to map the surface of an electrode recovered from a partially charged

DOI: 10.1021/acs.chemmater.6b05114
Chem. Mater. 2017, 29, 3347−3362

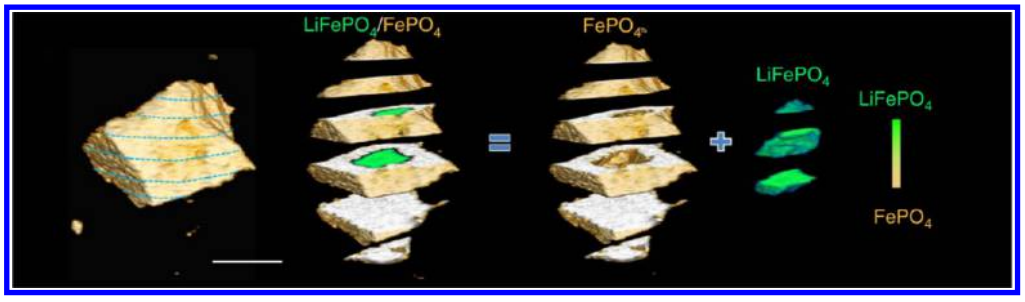

Figure 12. Sliced view of $LiFePO_4$ at a highly delithiated state. The sliced view reveals 3D internal core−shell phase distribution. Scale bar, 10 μm. Reprinted from ref 23, licensed under CC-BY 4.0.

prismatic cell, shown in Figure 13. However, this work was carried out at coarse spatial resolutions (several μm), compared

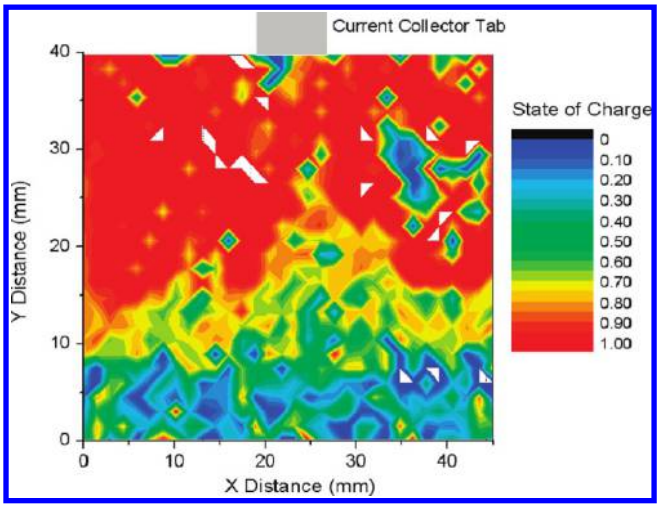

Figure 13. $FePO_4$ phase concentration profile of the prismatic electrode at 50% state-of-charge. Reprinted with permission from ref 57.

to the nanoscale resolution of the other microscopic mechanisms discussed in this Perspective. Nonetheless, valuable information was gathered at the scale of the whole electrode. Indeed, at high rates, they found a strong gradient in the phase distribution along the direction of current flow from the connector tab. The choice of a two-phase material ($LiFePO_4$) means the phase distribution within a large electrode is unlikely to change dramatically once the driving force is removed and the electrode is removed from the cell and therefore enabled the ex situ measurements to produce meaningful data.

Structural imaging is compatible with tomographic reconstruction. Jensen et al. analyzed coin-cell and 18650-cell batteries using tomography and high-energy diffraction.[58] Line scans were performed across the battery and at angles spanning 180° using a two-dimensional detector. The end result could *potentially* be a full two-dimensional diffraction pattern at every position on the reconstructed slice (Figure 14). In practice, the authors first integrated each projection pattern azimuthally to a one-dimensional diffractogram and then performed a reconstruction for each scattering vector length, q. The two-dimensional diffraction pattern contains texture and strain information that is lost when dimensionality is reduced.[59] This feature was exploited by the authors by separately integrating radially to map inhomogeneities in the preferred orientation of the $LiCoO_2$ cathode material. The 70 keV

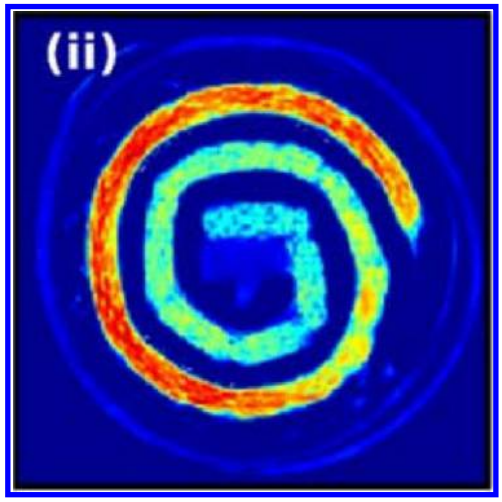

Figure 14. Data collected for cycled Ni-MH cell showing intensity at q = 1.36 $Å^{-1}$, representing the cathode phase.[58] Copyright 2015 The Authors. Published by ECS. Creative Commons Attribution 4.0 License (CC-BY). Full text: http://jes.ecsdl.org/content/162/7/A1310.full.

radiation used passes easily through the case material, allowing the measurements to be performed in situ (though not operando), avoiding any effects caused by disassembly of the cell.

The penetrating power of high energy X-rays can make for a very compelling operando experiment since the cell does not have to be modified, allowing conventional coin cells to be used. Strobridge et al. mapped the volume of a $LiFePO_4$ cathode in this way.[32] The incoming beam was scanned along the width and/or height of the cell while a collimator between the sample and the detector allowed the authors to discriminate which gauge volume along the beam was being probed (see Figure 15). The use of energy dispersive diffraction meant that the collimator did not limit the range of scattering vectors (q) being sampled. This feature allowed for direct mapping of the entire volume. With this technique, a clear relationship between electrode depth and state of charge was observed, leading to valuable conclusions about the rate-limiting steps in the reaction mechanism. They also uncovered inhomogeneities across the width of the electrode and used their measurements to validate a model exploring the effects of electrode porosity.

Using a microprobe of 1.7 μm, Zhang et al. probed individual nanoscale $LiFePO_4$ crystallites operando. Slight rotation of the sample illuminated several crystallites that satisfied the diffraction condition. Each crystallite was separately resolved because it was represented by a unique spot on the diffraction ring in the two-dimensional diffraction pattern. By following

DOI: 10.1021/acs.chemmater.6b05114
Chem. Mater. 2017, 29, 3347−3362

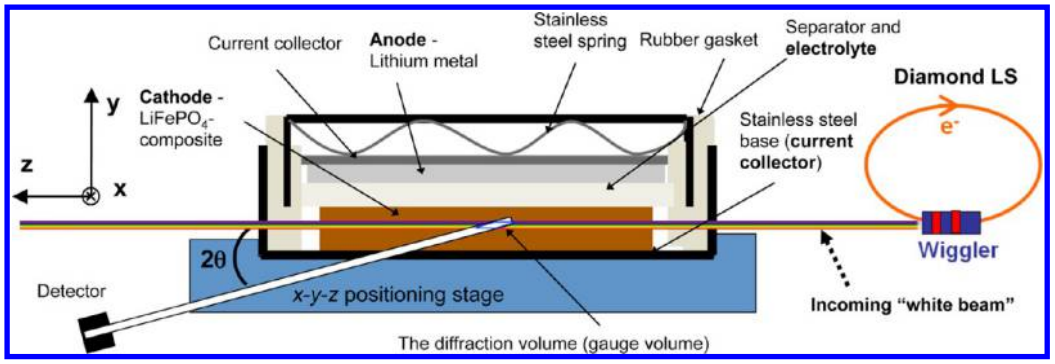

Figure 15. In situ EDXRD setup at the Diamond Light Source and the cross section of a coin-cell battery placed on an $x-y-z$ position stage. X-rays penetrate the stainless steel casing and the diffracted X-rays are detected at a fixed angle. Reprinted with permission from ref 32.

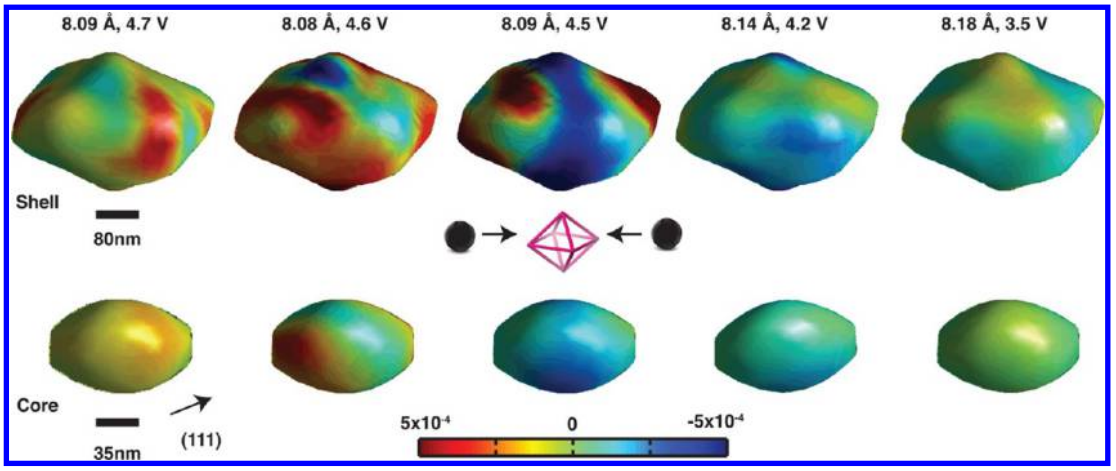

Figure 16. Isosurface projections of strain evolution in $LiNi_{0.5}Mn_{1.5}O_4$ nanoparticle. The shell and core both show inhomogeneous strain during discharge. Images are labeled by their respective lattice constant values and open circuit voltages. The highest lattice strain occurs immediately prior to the phase transformation. Reprinted with permission from ref 63.

each of those spots through (dis)charge, the homogeneity and nature of the phase transformation was examined. They found that at a slower rate of (dis)charge the phase transformation occurs more homogeneously and gradually, while faster rates see the advent of defined phase boundaries.[60]

A similar strategy, relying on resolving crystallites through unique diffraction spots in the Debye ring, was also applied to *coherent* Bragg diffraction, this time using $LiNi_{0.5}Mn_{1.5}O_4$ as the case study.[61] The power of this contrast mode, however, is exemplified by studies where phenomena within a particle are resolved through reconstructions of the three-dimensional volume, known as *coherent diffraction imaging* (CDI). The specifics of the technique are also well suited to mapping strain within the particle. Ulvestad et al. released a series of papers using this technique. They first demonstrated its validity by mapping the strain and displacement of material within a particle.[62] The strain evolution of $LiNi_{0.5}Mn_{1.5}O_4$ was studied during charge/discharge, and it was shown that significant gradients exist right before the phase transformation, shown in Figure 16.[63] In a separate experiment, they used strain maps to infer the existence of crystallographic defects within the crystallite and observed that these defects move as a function of charge state.[64] They were able to characterize the dislocation by studying the displacement field around it. Additionally, they quantified strain anisotropy, leading to the proposal of a hinge-like structure between the unit-cell layers that moves more freely once sufficient lithium is removed. On the basis of similar observations made during discharge, it was shown that an initial lithium-rich phase expands throughout the particle, rather than multiple nucleation sites appearing; this result suggests that, within a single particle, the reaction pathway was close to thermodynamic equilibrium in the conditions employed.

FUTURE OUTLOOK

The impact that X-ray imaging and mapping have already had in our understanding of electrochemical reactions relevant to batteries is significant. This Perspective demonstrates that it is currently possible to resolve chemical phenomena at the level of individual particles, at resolutions as low as 10 nm, and, in some cases, while the material is subject to working conditions. However, the wealth of techniques presented here and the incipience of these approaches lead to the conclusion that researchers are only beginning to exploit the information that can be collected. We have emphasized the importance of appropriately defining the goals of the experiment in terms of chemical, spatial, and temporal resolution. The three cannot currently be attained at the same time in an experiment that is directly relevant to function, with compromises leading to loss of chemical information in most cases. It is also important to recognize and understand the interaction between the beam and the material, especially when molecules sensitive to radiation, such as the organic solvents in a battery electrolyte, are present. This understanding is currently extremely rudimentary, so systematic studies should be incentivized.

DOI: 10.1021/acs.chemmater.6b05114
Chem. Mater. 2017, 29, 3347−3362

When it comes to operando measurements, further improvements in measurement protocols and cell design are necessary. Data analysis "on the fly" would provide valuable input to the experimenter in terms of defining the chances of success of the experiment and creating options for data minimization and experiment optimization. When it comes to experimental environments, the higher the resolution desired, the heavier the need for engineering cells that notably differ from conventional battery setups such as coin or even prismatic cells. This design often imposes conditions that are not representative or where quantitative electroanalysis simultaneous to the observations is not possible, inducing a critical loss of information. Further, given the ultimate goal of guiding improvements in battery performance, it is important that the design of operando cells takes into account the need to preserve the fidelity of the electrochemical responses to those that define function in a device.

As the community increases its awareness of the unique capabilities of X-ray microscopes, it is expected that their use in battery research will continue to grow. Since chemical imaging is only possible at a synchrotron, this growth will contribute to a vibrant and diverse user community. The fact that synchrotron scientists continue to improve existing setups and design new modes of imaging will contribute to the presence of X-ray chemical imaging and mapping in battery research. In this context, the availability of access to the synchrotron facilities where the measurements are performed is likely to become an even more pronounced limiting factor to be tackled by the agencies managing the facilities. A solution would involve improvements in the flux and brightness of the X-ray source to decrease measurement times. Indeed, many facilities are in the process of upgrading their storage rings to provide X-rays to enable techniques with increased complexity, while shortening the measurement times for those that are already possible today. The National Synchrotron Light Source II (NSLS-II) has now replaced the original NSLS at Brookhaven. Additionally, the Advanced Photon Source (APS), Advanced Light Source, Stanford Synchrotron Radiation Lightsource, and Cornell High Energy Synchrotron Source (United States), as well as Deutsches Elektronen-Synchrotron and European Synchrotron Radiation Facility in Europe, and SPring-8 in Japan all have plans for upgrading in the future, though many of these are still in very early planning stages. These improvements promise brighter and more coherent X-rays. The APS-U project also promises X-ray beams that will be much smaller in the horizontal direction, allowing more of the beam to be focused on the sample for imaging applications. The coherence of the X-rays is critical for ptychography and CDI; having pervasive access to coherent radiation will make these imaging techniques faster and more efficient than today. Increased brightness will shorten the time needed to acquire a data set of sufficient quality for analysis. These developments would bring experiments without compromises in any of the dimensions of resolution closer to reality. In other words, it would translate into an increase in the time resolution of operando experiments without sacrificing spatial or chemical resolution and will facilitate the next generation of high-impact experiments. Both operando and three-dimensional analyses have demonstrated their ability to generate insights that would otherwise go unnoticed: combining them in a robust and practical way will likely be at the forefront of battery imaging techniques. These developments will surely drastically improve the way that we are able to define relevant reactions, at the level of molecules to architectures, providing vital inputs for the design of devices that break current barriers of performance.

AUTHOR INFORMATION

Corresponding Author

*E-mail jcabana@uic.edu.

ORCID

Jordi Cabana: 0000-0002-2353-5986

Notes

The authors declare no competing financial interest.

Biographies

Mark Wolf is a Ph.D. candidate at the University of Illinois at Chicago performing research on cathode materials using ptychography and operando X-ray microscopy. He received a Bachelor of Science from Western Michigan University in 2008 with a dual major in chemistry and music.

Brian May is a Ph.D. candidate at the University of Illinois at Chicago in Dr. Jordi Cabana's group. Prior to his time at UIC, he received his B.S. in chemistry from Loyola University at Chicago in 2013 and researched allosteric activation mechanisms and protein crystal structures with Dr. Miguel Ballicora and Dr. Dali Liu. His current research focuses on developing new synchrotron techniques for applications in understanding the chemical reactions of battery cathode materials.

Jordi Cabana is an Assistant Professor at the Department of Chemistry of the University of Illinois at Chicago. Prior to his appointment at UIC, he was a Research Scientist at Lawrence Berkeley National Laboratory (U.S.A.), from 2008 until 2013. Prof. Cabana completed his Ph.D. in Materials Science at the Institut de Ciència de Materials de Barcelona (Spain) in 2004 and worked in the Department of Chemistry at Stony Brook University (U.S.A.) as a postdoctoral associate. He is generally interested in the physical and inorganic chemistry of materials, with emphasis on their redox and transport properties and a focus on applications in electrochemical energy storage. Members of his group are frequent users of synchrotron techniques such as diffraction, spectroscopy, and microscopy.

ACKNOWLEDGMENTS

This work was supported as part of the NorthEast Center for Chemical Energy Storage (NECCES), an Energy Frontier Research Center, funded by the U.S. Department of Energy, Office of Science, Basic Energy Sciences, under Award No. DE-SC0012583.

REFERENCES

(1) Whittingham, M. S. History, Evolution, and Future Status of Energy Storage. *Proc. IEEE* **2012**, *100*, 1518−1534.

(2) Armand, M.; Tarascon, J.-M. Building Better Batteries. *Nature* **2008**, *451*, 652−657.

(3) Newman, J. Optimization of Porosity and Thickness of a Battery Electrode by Means of a Reaction-Zone Model. *J. Electrochem. Soc.* **1995**, *142*, 97−101.

(4) Wu, S.-L.; Javier, A. E.; Devaux, D.; Balsara, N. P.; Srinivasan, V. Discharge Characteristics of Lithium Battery Electrodes with a Semiconducting Polymer Studied by Continuum Modeling and Experiment. *J. Electrochem. Soc.* **2014**, *161*, A1836−A1843.

(5) Palacin, M. R. Recent Advances in Rechargeable Battery Materials: A Chemist's Perspective. *Chem. Soc. Rev.* **2009**, *38*, 2565−2575.

DOI: 10.1021/acs.chemmater.6b05114
Chem. Mater. 2017, 29, 3347−3362

(6) Holt, M.; Harder, R.; Winarski, R.; Rose, V. Nanoscale Hard X-Ray Microscopy Methods for Materials Studies. *Annu. Rev. Mater. Res.* **2013**, *43*, 183−211.
(7) Maire, E.; Withers, P. J. Quantitative X-ray tomography. *Int. Mater. Rev.* **2014**, *59*, 1−43.
(8) Chae, S. R.; Moon, J.; Yoon, S.; Bae, S.; Levitz, P.; Winarski, R.; Monteiro, P. J. M. Advanced Nanoscale Characterization of Cement Based Materials Using X-Ray Synchrotron Radiation: A Review. *Int. J. Concr. Struct. Mater.* **2013**, *7*, 95−110.
(9) Tsuji, K.; Matsuno, T.; Takimoto, Y.; Yamanashi, M.; Kometani, N.; Sasaki, Y. C.; Hasegawa, T.; Kato, S.; Yamada, T.; Shoji, T.; Kawahara, N. New Developments of X-ray Fluorescence Imaging Techniques in Laboratory. *Spectrochim. Acta, Part B* **2015**, *113*, 43−53.
(10) Shapiro, D. A.; Yu, Y.-S.; Tyliszczak, T.; Cabana, J.; Celestre, R.; Chao, W.; Kaznatcheev, K.; Kilcoyne, D. A. L.; Maia, F.; Marchesini, S.; Meng, Y. S.; Warwick, T.; Yang, L. L.; Padmore, H. A. Chemical Composition Mapping with Nanometre Resolution by Soft X-ray Microscopy. *Nat. Photonics* **2014**, *8*, 765−769.
(11) Guinebretière, R. *X-ray Diffraction by Polycrystalline Materials*; ISTE Ltd.: 2007; pp 39−48.
(12) Mobilio, S.; Boscherini, F.; Meneghini, C. *Synchrotron Radiation*; Springer-Verlag: Berlin, Heidelberg, 2015.
(13) Ice, G. E.; Pang, J. W. Tutorial on x-ray microLaue diffraction. *Mater. Charact.* **2009**, *60*, 1191−1201.
(14) Snigirev, A.; Kohn, V.; Snigireva, I.; Lengeler, B. A compound refractive lens for focusing high-energy X-rays. *Nature* **1996**, *384*, 49−51.
(15) Kirkpatrick, P.; Baez, A. V. Formation of Optical Images by X-Rays. *J. Opt. Soc. Am.* **1948**, *38*, 766−774.
(16) Fresnel Zone Plate Theory. http://zoneplate.lbl.gov/theory (accessed Nov. 4, 2016).
(17) Yan, H.; Conley, R.; Bouet, N.; Chu, Y. S. Hard x-ray Nanofocusing by Multilayer Laue Lenses. *J. Phys. D: Appl. Phys.* **2014**, *47*, 263001.
(18) Meirer, F.; Cabana, J.; Liu, Y.; Mehta, A.; Andrews, J.; Pianetta, P. Three-dimensional Imaging of Chemical Phase Transformations at the Nanoscale with Full-Field Transmission X-ray Microscopy. *J. Synchrotron Radiat.* **2011**, *18*, 773−781.
(19) Li, Y.; Weker, J. N.; Gent, W. E.; Mueller, D. N.; Lim, J.; Cogswell, D. A.; Tyliszczak, T.; Chueh, W. C. Dichotomy in the Lithiation Pathway of Ellipsoidal and Platelet $LiFePO_4$ Particles Revealed through Nanoscale Operando State-of-Charge Imaging. *Adv. Funct. Mater.* **2015**, *25*, 3677−3687.
(20) Farmand, M.; et al. Near-Edge X-ray Refraction Fine Structure Microscopy. *Appl. Phys. Lett.* **2017**, *110*, 063101.
(21) Li, L.; Chen-Wiegart, Y.-c. K.; Wang, J.; Gao, P.; Ding, Q.; Yu, Y.-S.; Wang, F.; Cabana, J.; Wang, J.; Jin, S. Visualization of Electrochemically Driven Solid-State Phase Transformations Using Operando Hard X-ray Spectro-imaging. *Nat. Commun.* **2015**, *6*, 6883.
(22) Yin, G.-C.; Tang, M.-T.; Song, Y.-F.; Chen, F.-R.; Liang, K. S.; Duewer, F. W.; Yun, W.; Ko, C.-H.; Shieh, H.-P. D. Energy-tunable Transmission X-ray Microscope for Differential Contrast Imaging with Near 60 nm Resolution Tomography. *Appl. Phys. Lett.* **2006**, *88*, 241115.
(23) Wang, J.; Karen Chen-Wiegart, Y.-C.; Eng, C.; Shen, Q.; Wang, J. Visualization of Anisotropic-Isotropic Phase Transformation Dynamics in Battery Electrode Particles. *Nat. Commun.* **2016**, *7*, 12372.
(24) Yu, Y.-S.; et al. Dependence on Crystal Size of the Nanoscale Chemical Phase Distribution and Fracture in Li_xFePO_4. *Nano Lett.* **2015**, *15*, 4282−4288.
(25) Shlens, J. A Tutorial on Independent Component Analysis. https://arxiv.org/abs/1404.2986 (accessed Aug. 13, 2016).
(26) Knuth, K. H. Informed Source Separation: A Bayesian Tutorial. https://arxiv.org/abs/1311.3001 (accessed Aug. 13, 2016).
(27) Bioucas-Dias, J. M.; Plaza, A. An overview on hyperspectral unmixing: Geometrical, statistical, and sparse regression based approaches. *GeoScience and Remote Sensing Symposium (IGARSS), 2011 IEEE International*; IEEE: 2011; pp 1135−1138.
(28) Duarte, L. T.; Moussaoui, S.; Jutten, C. Source Separation in Chemical Analysis: Recent achievements and perspectives. *IEEE Signal Processing Magazine* **2014**, *31*, 135−146.
(29) Boesenberg, U.; Meirer, F.; Liu, Y.; Shukla, A.; Dell'Anna, R.; Tyliszczak, T.; Chen, G.; Andrews, J.; Richardson, T.; Kostecki, R.; Cabana, J. Mesoscale Phase Distribution in Single Particles of $LiFePO_4$ following Lithium Deintercalation. *Chem. Mater.* **2013**, *25*, 1664−1672.
(30) Deb, A.; Cairns, E. J. In Situ X-ray Absorption Spectroscopy - A Probe of Cathode Materials for Li-Ion Cells. *Fluid Phase Equilib.* **2006**, *241*, 4−19.
(31) Kämpfe, B.; Luczak, F.; Michel, B. Energy Dispersive X-Ray Diffraction. *Part. Part. Syst. Charact.* **2005**, *22*, 391−396.
(32) Strobridge, F. C.; Orvananos, B.; Croft, M.; Yu, H.-C.; Robert, R.; Liu, H.; Zhong, Z.; Connolley, T.; Drakopoulos, M.; Thornton, K.; Grey, C. P. Mapping the Inhomogeneous Electrochemical Reaction Through Porous $LiFePO_4$-Electrodes in a Standard Coin Cell Battery. *Chem. Mater.* **2015**, *27*, 2374−2386.
(33) Robinson, I.; Harder, R. Coherent X-ray diffraction imaging of strain at the nanoscale. *Nat. Mater.* **2009**, *8*, 291−298.
(34) Venkatakrishnan, S. V.; Farmand, M.; Yu, Y. S.; Majidi, H.; van Benthem, K.; Marchesini, S.; Shapiro, D. A.; Hexemer, A. Robust X-Ray Phase Ptycho-Tomography. *IEEE Signal Processing Letters* **2016**, *23*, 944−948.
(35) Liu, H.; Strobridge, F. C.; Borkiewicz, O. J.; Wiaderek, K. M.; Chapman, K. W.; Chupas, P. J.; Grey, C. P. Capturing Metastable Structures During High-Rate Cycling of LiFePO4 Nanoparticle Electrodes. *Science* **2014**, *344*, 1252817.
(36) Lim, J.; Li, Y.; Alsem, D. H.; So, H.; Lee, S. C.; Bai, P.; Cogswell, D. A.; Liu, X.; Jin, N.; Yu, Y.-s.; Salmon, N. J.; Shapiro, D. A.; Bazant, M. Z.; Tyliszczak, T.; Chueh, W. C. Origin and hysteresis of lithium compositional spatiodynamics within battery primary particles. *Science* **2016**, *353*, 566−571.
(37) Borkiewicz, O. J.; Wiaderek, K. M.; Chupas, P. J.; Chapman, K. W. Best Practices for Operando Battery Experiments: Influences of X-ray Experiment Design on Observed Electrochemical Reactivity. *J. Phys. Chem. Lett.* **2015**, *6*, 2081−2085.
(38) Lin, C.-K.; Ren, Y.; Amine, K.; Qin, Y.; Chen, Z. In Situ High-Energy X-ray Diffraction to Study Overcharge Abuse of 18650-size Lithium-Ion Battery. *J. Power Sources* **2013**, *230*, 32−37.
(39) Borkiewicz, O. J.; Shyam, B.; Wiaderek, K. M.; Kurtz, C.; Chupas, P. J.; Chapman, K. W. The AMPIX Electrochemical Cell: a Versatile Apparatus for In Situ X-ray Scattering and Spectroscopic Measurements. *J. Appl. Crystallogr.* **2012**, *45*, 1261−1269.
(40) Whittingham, M. S. Ultimate Limits to Intercalation Reactions for Lithium Batteries. *Chem. Rev.* **2014**, *114*, 11414−11443.
(41) Balogun, M.-S.; Qiu, W.; Luo, Y.; Meng, H.; Mai, W.; Onasanya, A.; Olaniyi, T. K.; Tong, Y. A review of the development of full cell lithium-ion batteries: The impact of nanostructured anode materials. *Nano Res.* **2016**, *9*, 2823−2851.
(42) Finegan, D. P.; Scheel, M.; Robinson, J. B.; Tjaden, B.; Hunt, I.; Mason, T. J.; Millichamp, J.; Di Michiel, M.; Offer, G. J.; Hinds, G.; Brett, D. J. L.; Shearing, P. R. In-operando high-speed tomography of lithium-ion batteries during thermal runaway. *Nat. Commun.* **2015**, *6*, 6924.
(43) Eastwood, D.; Bradley, R.; Tariq, F.; Cooper, S.; Taiwo, O.; Gelb, J.; Merkle, A.; Brett, D.; Brandon, N.; Withers, P.; Lee, P.; Shearing, P. The application of phase contrast X-ray techniques for imaging Li-ion battery electrodes. *Nucl. Instrum. Methods Phys. Res., Sect. B* **2014**, *324*, 118−123.
(44) Cooper, S.; Eastwood, D.; Gelb, J.; Damblanc, G.; Brett, D.; Bradley, R.; Withers, P.; Lee, P.; Marquis, A.; Brandon, N.; Shearing, P. Image based modelling of microstructural heterogeneity in $LiFePO_4$ electrodes for Li-ion batteries. *J. Power Sources* **2014**, *247*, 1033−1039.
(45) Cabana, J.; Monconduit, L.; Larcher, D.; Palacín, M. R. Beyond Intercalation-Based Li-Ion Batteries: The State of the Art and Challenges of Electrode Materials Reacting Through Conversion Reactions. *Adv. Mater.* **2010**, *22*, E170−E192.

DOI: 10.1021/acs.chemmater.6b05114
Chem. Mater. 2017, 29, 3347−3362

(46) Ebner, M.; Marone, F.; Stampanoni, M.; Wood, V. Visualization and Quantification of Electrochemical and Mechanical Degradation in Li Ion Batteries. *Science* **2013**, *342*, 716−720.
(47) Wang, J.; Chen-Wiegart, Y.-c. K.; Wang, J. In Situ Three-Dimensional Synchrotron X-Ray Nanotomography of the (De)-lithiation Processes in Tin Anodes. *Angew. Chem., Int. Ed.* **2014**, *53*, 4460−4464.
(48) Yang, F.; Liu, Y.; Martha, S. K.; Wu, Z.; Andrews, J. C.; Ice, G. E.; Pianetta, P.; Nanda, J. Nanoscale Morphological and Chemical Changes of High Voltage Lithium-Manganese Rich NMC Composite Cathodes with Cycling. *Nano Lett.* **2014**, *14*, 4334−4341.
(49) Lin, F.; Nordlund, D.; Li, Y.; Quan, M. K.; Cheng, L.; Weng, T.-C.; Liu, Y.; Xin, H. L.; Doeff, M. M. Metal segregation in hierarchically structured cathode materials for high-energy lithium batteries. *Nat. Energy* **2016**, *1*, 15004.
(50) Xu, J.; Lin, F.; Doeff, M. M.; Tong, W. A review of Ni-based layered oxides for rechargeable Li-ion batteries. *J. Mater. Chem. A* **2017**, *5*, 874−901.
(51) Wang, J.; Chen-Wiegart, Y.-c. K.; Wang, J. In situ Chemical Mapping of a Lithium-Ion Battery Using Full-Field Hard X-ray Spectroscopic Imaging. *Chem. Commun.* **2013**, *49*, 6480−6482.
(52) Ohzuku, T.; Kitagawa, M.; Hirai, T. Electrochemistry of Manganese Dioxide in Lithium Nonaqueous Cell. *J. Electrochem. Soc.* **1990**, *137*, 769−775.
(53) Yu, Y.-S.; Kim, C.; Liu, Y.; van der Ven, A.; Meng, Y. S.; Kostecki, R.; Cabana, J. Nonequilibrium Pathways during Electrochemical Phase Transformations in Single Crystals Revealed by Dynamic Chemical Imaging at Nanoscale Resolution. *Adv. Energy Mater.* **2015**, *5*, 1402040.
(54) Wang, J.; Chen-Wiegart, Y.-c. K.; Wang, J. In Operando Tracking Phase Transformation Evolution of Lithium Iron Phosphate with Hard X-ray Microscopy. *Nat. Commun.* **2014**, *5*, 4570.
(55) Olivares-Marín, M.; Sorrentino, A.; Lee, R.-C.; Pereiro, E.; Wu, N.-L.; Tonti, D. Spatial Distributions of Discharged Products of Lithium-Oxygen Batteries Revealed by Synchrotron X-ray Transmission Microscopy. *Nano Lett.* **2015**, *15*, 6932−6938.
(56) Woodford, W.; Carter, W.; Chiang, Y. Design criteria for electrochemical shock resistant battery electrodes. *Energy Environ. Sci.* **2012**, *5*, 8014−8024.
(57) Liu, J.; Kunz, M.; Chen, K.; Tamura, N.; Richardson, T. Visualization of Charge Distribution in a Lithium Battery Electrode. *J. Phys. Chem. Lett.* **2010**, *1*, 2120−2123.
(58) Jensen, K. M. Ø.; Yang, X.; Laveda, J. V.; Zeier, W. G.; See, K. A.; Michiel, M. D.; Melot, B. C.; Corr, S. A.; Billinge, S. J. L. X-Ray Diffraction Computed Tomography for Structural Analysis of Electrode Materials in Batteries. *J. Electrochem. Soc.* **2015**, *162*, A1310−A1314.
(59) He, B. B. *Two-Dimensional X-Ray Diffraction*; John Wiley & Sons, Inc.: 2009; pp 219−249.
(60) Zhang, X.; van Hulzen, M.; Singh, D. P.; Brownrigg, A.; Wright, J. P.; van Dijk, N. H.; Wagemaker, M. Direct View on the Phase Evolution in Individual $LiFePO_4$ Nanoparticles During Li-ion Battery Cycling. *Nat. Commun.* **2015**, *6*, 8333.
(61) Singer, A.; Ulvestad, A.; Cho, H.-M.; Kim, J. W.; Maser, J.; Harder, R.; Meng, Y. S.; Shpyrko, O. G. Nonequilibrium Structural Dynamics of Nanoparticles in $LiNi_{1/2}Mn_{3/2}O_4$ Cathode under Operando Conditions. *Nano Lett.* **2014**, *14*, 5295−5300.
(62) Ulvestad, A.; Cho, H. M.; Harder, R.; Kim, J. W.; Dietze, S. H.; Fohtung, E.; Meng, Y. S.; Shpyrko, O. G. Nanoscale Strain Mapping in Battery Nanostructures. *Appl. Phys. Lett.* **2014**, *104*, 073108.
(63) Ulvestad, A.; Singer, A.; Cho, H.-M.; Clark, J. N.; Harder, R.; Maser, J.; Meng, Y. S.; Shpyrko, O. G. Single Particle Nanomechanics in Operando Batteries via Lensless Strain Mapping. *Nano Lett.* **2014**, *14*, 5123−5127.
(64) Ulvestad, A.; Singer, A.; Clark, J. N.; Cho, H. M.; Kim, J. W.; Harder, R.; Maser, J.; Meng, Y. S.; Shpyrko, O. G. Topological Defect Dynamics in Operando Battery Nanoparticles. *Science* **2015**, *348*, 1344−1347.

DOI: 10.1021/acs.chemmater.6b05114
Chem. Mater. 2017, 29, 3347−3362